Nanomechanical Spectroscopy of Synthetic and Biological Membranes

Journal:	*Nanoscale*
Manuscript ID:	NR-ART-05-2013-002643.R1
Article Type:	Paper
Date Submitted by the Author:	25-Mar-2014
Complete List of Authors:	Lu, Junhong; Shanghai Institute of Applied Physics, Yang, Ju; Columbia University, Biological Sciences Dong, Mingdong; Aarhus University, Sahin, Ozgur; Columbia University,

SCHOLARONE™
Manuscripts

Journal Name

Dynamic Article Links ▶

ARTICLE TYPE

Nanomechanical Spectroscopy of Synthetic and Biological Membranes

Junhong Lü,[a,b] **Ju Yang**[c]**, Mingdong Dong**[a,d] **and Ozgur Sahin***[c,e]

5 We report that atomic force microscopy based high-speed nanomechanical analysis can identify components of complex heterogeneous synthetic and biological membranes from the measured spectrum of nanomechanical properties. We have investigated phase separated ternary lipid bilayers and purple membranes of *Halobacterium salinarum*. The nanomechanical spectra recorded on these samples identify all membrane components, some of which are difficult to resolve in conventional phase images. This non-destructive approach can aid the design of synthetic lipid bilayers and studies lateral organization of complex heterogeneous cellular membranes.

10

Introduction

Lateral organization of lipid and protein components within membranes is involved in numerous cellular events such as signal transduction and membrane fusion during viral entry.[1-6]
15 Therefore, identifying chemical components in a spatially resolved manner can provide new insights into membrane organization and function.[2,3,7] Present knowledge of the lateral organization of synthetic and biological membrane accumulated mostly from fluorescence and electron microscopy methods.[8,9]
20 Atomic force microscopy (AFM) has complemented these methods due to its ability to image membranes with high spatial resolution under close to native conditions.[2,6,10-17] Multiple-frequency AFM techniques provide new opportunities for mapping and identifying compositions of synthetic and biological
25 membranes in detail.[18-27] These developments mainly rely on excitation and/or detection of AFM cantilever oscillations at multiple frequencies,[28] which allow making detailed mechanical measurements with high sensitivity and speed. Images based on higher-harmonic vibrations,[22,23,29] torsional vibrations,[30,31] bi-
30 modal[32] and broadband excitation detection[33] of the cantilever vibrations have been successfully employed to study biological samples including isolated proteins,[34-36] membranes,[20-24,29,37-39] viruses[21,40] and cells.[41-43] The improved speed, spatial resolution, and sensitivity in mechanical measurements can potentially allow
35 discrimination of chemical components of membranes with gentle forces, because different molecular components and physical states are likely to create significant variations in local mechanical properties.

In this study, we explored this possibility by using
40 microsecond force spectroscopy[36] (µFS), which relies on T-shaped cantilevers that twist in response to high-speed tip-sample interaction forces during dynamic AFM imaging. We measured the spectra of mechanical properties of heterogeneous synthetic and biological membranes that showed peaks sufficiently distinct
45 to allow discrimination of multiple components simultaneously. Although components of binary lipid systems incorporating a fluid and a gel phase can be distinguished in conventional AFM based mechanical images, multiple components have proven

difficult to resolve. Our results show that mechanical
50 measurements with µFS allow analysis of complex heterogeneous membranes to identify their components and lateral organization in a non-destructive manner.

µFS relies on time-resolved tip-sample force measurements in fluid tapping-mode AFM.[36] The cantilever typically oscillates
55 at a frequency close to 10 KHz, which results in a period of oscillations close 100 µs. Due to the intermittent contacts between the tip and the sample, pulse-like forces acting on the tip exhibit even shorter durations, typically around 10-20 µs. Resolving these force waveforms is made difficult by the limited
60 mechanical bending of the cantilever. The high bandwidths of the twisting motion of T-shaped cantilevers used in µFS allow measuring these forces with microsecond time resolution. High speed force-distance curves are obtained by measuring forces from the twist angle and distances from the vertical deflection of
65 the cantilever. These curves can be analyzed using physical models describing tip-sample interactions to measure a variety of local material properties. It is possible to carry out these calculations in real-time while the cantilever is scanning the surface, so that mechanical property images can be produced in
70 parallel to the conventional topography and phase images of fluid tapping mode.

Experimental

Materials: DOPC (1,2-dioleoyl-sn-glycero-3-phosphocholine), DPPC (1,2-dipalmitoyl-sn-glycero- 3-phosphocholine) and DPPE
75 (1,2-dipalmitoyl-sn-glycero-3-phosphoethanolamine) were purchased from Avanti Polar Lipids Inc., Alabaster, AL.
Preparation and AFM observation of phase separated lipid bilayer (SLBs): SLBs were prepared using the fusion method of small unilamellar vesicles (SUVs). Lipids dissolved in
80 chloroform are first dried under argon, then resuspended in methylene chloride and re-evaporated three times. After gently swirling phosphate buffered saline(PBS) over the dried lipid, SUVs were synthesized by sonication in a bath sonicator (Laboratory Supplies Co., Hicksville, NY) until the suspension
85 was visually clear. A sufficient amount of the SUV solution is incubated with freshly cleaved mica for 30 min at the temperature

ARTICLE TYPE
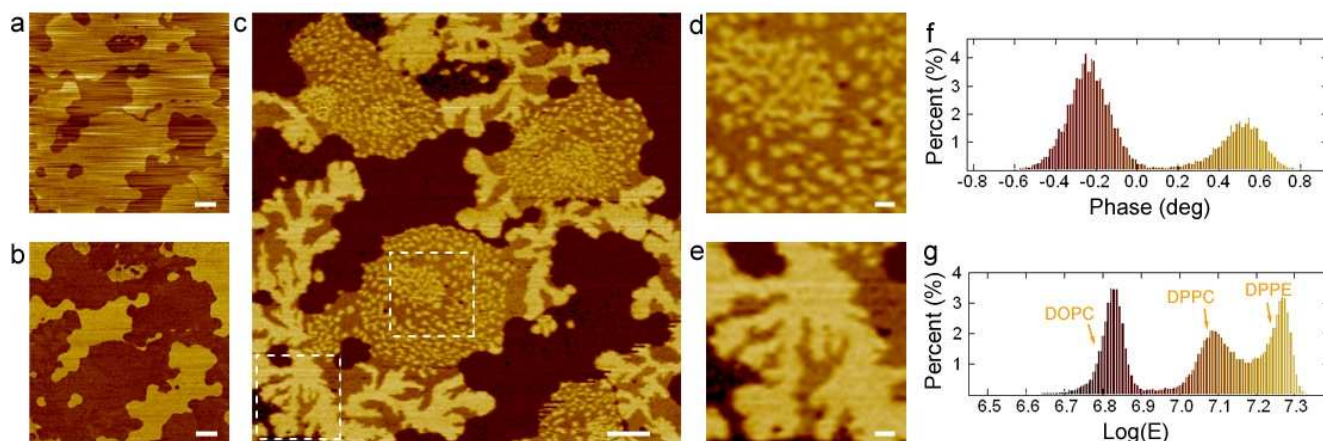
Fig. 1 Nanomechanical spectroscopy of a ternary lipid bilayer. The effective elastic modulus map (c) is generated simultaneously with topography (a) and phase (b) images. Scale bars: 500 nm. The effective elastic modulus map shows surface features that are not seen in phase or topography images. The areas marked with dashed rectangles in (c) are magnified in (d,e). Scale bars: 100 nm. The Histograms of the values in phase (b) and effective elastic
5 modulus (c) images are given in (f) and (g), respectively. The bars in histograms are colored to match corresponding images. Logarithm of effective elastic modulus (E) values are calculated when E is given in the unit of Pa.

above the transition temperature (Tm) and then slowly cooled down to room temperature. AFM measurements were carried out under PBS buffer.

10 **Preparation of purple membranes for AFM imaging:** Purple membrane of *H. salinarum* (Sigma-Aldrich) was suspended in a stock solution of ultrapure water and diluted to 50µg ml^{-1}, in an adsorption buffer (300 mM KCl, 10mM Tris/HCl, at pH 7.8). The solution (10µl) was placed onto cleaved mica for 30min to allow
15 membrane absorption on the surface. Measurements were carried out under the same buffer conditions. Detailed protocols for AFM imaging and spectroscopy of native purple membranes can be found in Müller and Engel[44].

AFM cantilevers: Two types of T-shaped cantilevers are used.
20 Both cantilevers are fabricated by using conventional manufacturing protocols (Applied Nanostructures and MikroMasch) with custom geometry. Electron microscope images of these cantilevers are given in previous reports [36,45]. The body of the first cantilever is made of silicon nitride and the
25 wider region at the free end including the tip is made of silicon. The cantilever is 130 µm long and 35 µm wide. The width at the free end is 55 µm. The tip offset distance is 22 µm. The thickness of the silicon nitride is 600 nm. The thickness of the silicon part is ~1 µm. The second cantilever is 300 µm long, 20 µm wide and
30 2.0 µm thick. The tip offset distance is 25 µm. The free end of the cantilever is 60 µm wide.

Results and Discussions

We have investigated the compositions and lateral organizations of a heterogeneous synthetic membrane and a
35 biological membrane using microsecond force spectroscopy. The synthetic membrane is a supported lipid bilayer composed of 1,2-dioleoyl-sn-glycero-3-phosphocholine (DOPC), 1,2-dipalmitoyl-sn-glycero-3-phosphocholine (DPPC) and 1,2-dipalmitoyl-sn-glycero-3-phosphoethanolamine (DPPE), prepared by vesicle
40 fusion method[46] and imaged on freshly cleaved mica substrate. Due to different melting temperatures, these lipids phase separate and create lateral heterogeneity within the bilayer. Furthermore, at room temperature, DOPC exhibits liquid-like phase, while DPPC and DPPE exhibit gel-like phase.

45 Figure 1 shows results of µFS based analysis of the ternary lipid bilayer. The topography and phase images shown in Figure 1a and 1b exhibit two-level response, despite the existence of three distinct molecular components of the bilayer. A histogram of the phase values showing two peaks is plotted in Figure 1f.
50 The two-levels can be attributed to gel-like and liquid-like phases within the bilayer. Previous reports on AFM based investigations of binary mixtures of liquid-like and gel-like phases showed that liquid phases is compressed more under the influence of tip-sample forces and therefore its apparent height is lowered.

55 Using µFS, we have calculated the local elastic modulus of the bilayer surface. Elastic modulus values are derived from the high-speed force-distance curves according to the DMT contact mechanics models. While accuracy of this model is limited to samples with homogenous and isotropic elastic properties near
60 the vicinity of the tip, the calculated values nevertheless provide a measure of local stiffness of the bilayer. Therefore, we will refer to these values as effective elastic moduli, hereafter.

Figure 1c shows the effective elastic modulus map of the lipid bilayer that is generated simultaneously with the topography (Fig.
65 1a) and phase images (Fig. 1b). The histogram of the elastic modulus values is given in Figure 1g. Different from the topography and phase images, the effective elastic modulus map reveals three distinct levels that correspond to all components of the ternary lipid bilayer. We attribute the lowest level (Log(E) ~
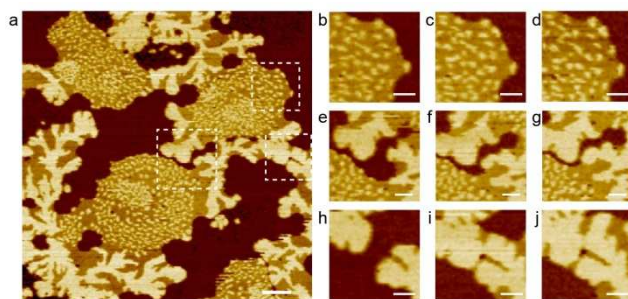
Fig. 2 Visualizing dynamic reorganization of the ternary lipid bilayer. Repeated scans of the ternary lipid bilayer show no apparent damage and thus allow visualizing dynamic reorganization of each of the three
5 components. The effective elastic modulus maps of the sample in Figure 1 are recorded in 15 min intervals. Time-dependent changes in three regions marked with dashed squares in (a) are given in (b-d) for the top rectangle, (e-g) for the center rectangle, and (h-j) for the rightmost rectangle. Scale bars: (a) 500 nm, (b-j) 200 nm.

10 6.8, E ~ 6.3 MPa) to DOPC due to its liquid-like behavior at room temperature, the middle level (Log(E) ~ 7.1, E ~ 12.6 MPa) to DPPC and the highest level (Log(E) ~ 7.3, E ~ 20.0 MPa) to DPPE. To verify assignments of elastic modulus values to the lipid domains, we have carried out additional experiments with
15 binary lipid bilayers and compared the elastic modulus values to the results of the ternary lipid bilayer in Fig. 1. Identifying the missing elastic modulus values in the binary system verified the assignments (see Fig. S1 of the electronic supplementary information). Note that DPPC can be expected to have a lower
20 effective elastic modulus vale than DPPE domains. Although DPPC and DPPE are both in the gel phase at room temperature, DPPC has a lower melting temperature than DPPE (41°C vs. 69°C) presumably due to the smaller headgroup of DPPE, which permits tighter packing of lipids. Furthermore, DPPE regions
25 appear to have two distinct lateral arrangements. Areas representative of these patterns are highlighted with dashed rectangles in Fig. 1c and magnified images are plotted in Fig. 1d,e. We suggest that the smaller domains in Fig. 1d could be the result of an intermediate step in phase separation of the lipid
30 mixture.

Because of the low tip-sample forces (peak tapping forces are kept below 200 pN), the imaging process is likely to result in little or no damage to the lipid bilayer. In agreement with this expectation, repeated images of the same surface area studied in
35 Figure 1 showed no apparent damage to the sample (Figure 2). This characteristic allows visualizing dynamic changes in the arrangement of each lipid component. Three examples highlighted in Figure 2(b-j) show regions of the surface exhibiting varying degrees of rearrangement. It is worth noting
40 that the small, ~50 nm sized, DPPE domains (brightest color) remain largely unchanged in Figure 2(b-d) and in Figure 2(e-g), whereas larger domains of DPPE and DPPC (light brown) go through substantial rearrangements in Figure 2(e-g) and in Figure 2(h-j). These kinds of observations can potentially lead to a better
45 understanding of forces governing the dynamics of complex lipid membranes.

Biological membranes can create more complicated situations than the synthetic lipid bilayer studied so far. As an example of a biological membrane, we have analyzed the effective elastic
50 modulus map observed on purple membranes *of Halobacterium*

salinarum. These membranes contain both lipid and protein components where proteins form two-dimensional crystalline domains. Lipids are found both in between bacteriorhodpsin trimers and in regions surrounding crystalline domains. The
55 surface created by depositing purple membranes on mica is complicated further by different orientations of the membranes (with cytoplasmic vs. extracellular surfaces on top) and by multiple layers deposited in the same region of the surface.
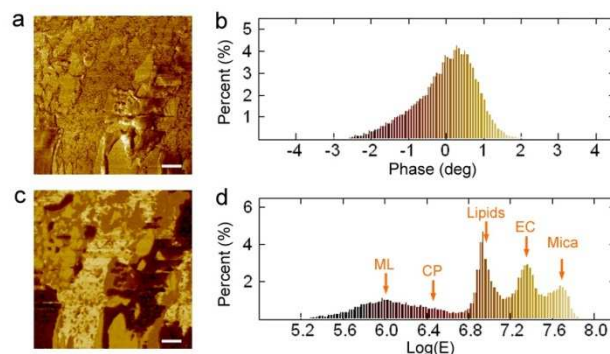
60 **Fig. 3** Nanomechanical spectroscopy of purple membranes. Although the phase image (a) exhibits noticeable contrast it is difficult to identify each component on the surface. The corresponding histogram (b) reveals little information as it shows only one peak. The effective elastic modulus map (c) exhibits five distinct color levels with clear boundaries, which are
65 marked on the corresponding histogram (d). The bars in histograms are colored to match corresponding images. Scale bars: 500nm. Logarithm of effective elastic modulus *(E)* values are calculated when E is given in the unit of Pa.

Figure 3 compares phase image and the effective elastic
70 modulus map of purple membranes deposited onto freshly cleaved mica. Although phase image in Figure 3a exhibits noticeable contrast, it is difficult to identify and assign material components forming the surface. This reflects onto the corresponding histogram in Figure 2b, which shows only one
75 peak. The effective elastic modulus map in Figure 3c exhibits five distinct color levels with clear boundaries. These color levels are marked on the corresponding histogram in Figure 3d. We attribute the regions with the lowest modulus (Log(E) ~ 6.0, **E** ~ 1.0 MPa) to multilayer membranes (ML) and the regions with
80 the highest modulus (Log(E) ~ 7.7, E ~ 50.1 MPa) to mica. To assign the remaining color levels to the cytoplasmic (CP) surfaces, extracellular (EC) surfaces, and lipids, we relied on previous measurements on the purple membrane, which showed that the EC side (Log(E) ~ 7.2, E ~ 15.8 MPa) is stiffer than the
85 CP side (Log(E) ~ 6.7, E ~ 5.0 MPa).[36] These previous measurements were done with the same type of cantilevers and same pH and ionic strength levels. Here we also observed that the lipids surrounding the crystalline regions formed by bacteriorhodopsin trimers exhibit an effective elastic modulus
90 between that of CP and EC regions (Log(E) ~ 6.9, E ~ 7.9 MPa).

Note that although one could expect the CP side to be more compliant than the EC side based on neutron scattering experiments[47] and the temperature factors in the crystal structure[48], we have carried out additional experiments with AFM
95 to provide further support for our assignments of elastic modulus values to the different sides of purple membranes. In these experiments, we relied on the difference in surface charge

densities between the EC and CP sides[49], which caused measurable height artifacts that are amplified at lower ionic strengths. Results in Fig. S2 of the electronic supplementary information show that the apparent height of the more compliant side of the membrane increases more than the stiff side of the membrane at lower ionic strengths of the imaging medium. This is in agreement with the higher surface charge density of the CP side[49]. It should be noted that it is possible to discriminate EC and CP sides in phase images by carefully choosing feedback conditions that enhances the contrast[50], however the presence of lipids and multiple layers complicate the assignment of components based on the measured phase values.

Conclusions

In summary, the demonstrated ability to resolve components of synthetic and biological membranes with µFS shows the potential of local mechanical properties in identifying chemical components of membranes. Although topography and phase images are affected by local mechanical properties, the coupling is indirect and their interpretation can be complicated if long range electrical forces and viscoelastic energy dissipation are present. By using multiple detection frequencies and reconstructing force distance curves, the µFS approach improves the resolving power of AFM substantially in determining components of complex heterogeneous membranes, thus providing a means for chemical identification at the nanoscale through mechanical measurements.

Acknowledgements

Notes and references

ᵃ The Rowland Institute at Harvard, Harvard University, Cambridge, MA, USA.
ᵇ Laboratory of Physical Biology, Shanghai Institute of Applied Physics, Shanghai 201800, China.
ᶜ Department of Biological Sciences, Columbia University, New York, NY 10027,USA
ᵈ Centre for DNA Nanotechnology (CDNA), Aarhus University, Aarhus C DK-8000, Denmark.
ᵉDepartment of Physics, Columbia University, New York, NY 10027,USA;
E-mail: sahin@columbia.edu

1. K.Simons and W. L.C.Vaz, *Annu. Rev. Biophys. Biomol. Struct.,* 2004, **33**, 269.
2. S.Semrau and T.Schmidt, *Soft Matter,* 2009, **5**, 3174.
3. D.Lingwood and K. Simons,*Science,* 2010,**327**,46.
4. S. Mayor and M.Rao, *Traffic,* 2004, **5**, 231.
5. L.Rajendran and K. Simons, *J. Cell Sci*., 2005, **118**, 1099.
6. J. Zhong, *Integr. Biol(Camb).,* 2011, **3**, 632.
7. J.Zimmerberg and K.Gawrisch, *Nature Chem. Biol.,* 2006, **11**,564.
8. R.G.W.Anderson and K. Jacobson, *Science,* 2002, **296**,1821.
9. S. Hess, M. Kumar, A. Verma, J. Farrington, A. Kenworthy and J. Zimmerberg, *J. Cell Biol.,* 2005, **169**,965.
10. K.K.Kirat, S.Morandat, and Y.F. Dufrêne, *Biochim. Biophys. Acta.-Biomembranes,* 2010,**1798**,750.
11. A. Alessabdrini and P. Facci, *J. Mol. Recognit.,* 2011, **24**,387.
12. EI.Goksu, J.M.Vanegas, C.D.Blanchette, W.C. Lin and M.L.Longo, *Biochim. Biophys. Acta.*, 2009, **1788**,254.
13. Y.F.Dufrêne,W.R.Barger,J.D.Green and G.U.Lee, *Langmuir,* 1997, **13**, 4779.
14. Z.V.Leonenko, E. Finot, H. Ma, T.E.S.Dahms and D.T.Cramb, *Biophys. J.,* 2004, **86**,3783.
15. L.J. Johnston, *Langmuir,* 2007*,* **23**, 5886.
16. S. Garcia-Manyes, L. Redondo-Morata, G. Oncins and F. Sanz, *J. Am. Chem. Soc.,* 2010,**132**, 12874.
17. N.Shamitko-Klingensmith, K. M. Molchanoff, K. A.Burke, G. J. Magnone and J.Legleiter, *Langmuir,* 2012,**28**,13411.
18. J.K Li,. R.M.Sullan, S.Zou, *Langmuir,* 2011, **27**,1308.
19. H.J.An, M. R. Nussio, M. G. Huson, N. H.Voelcker, and J.G.Shapter, *Biophys. J.,* 2010,**99**,834.
20. J. Preiner, J.Tang, V. Pastushenko, and P. Hinterdorfer, *Phys. Rev. Lett.*, 2007, **99**,046102.
21. J. Melcher, C.Carrasco, X. Xu, J.L.Carrascosa, J. Gomez-Herrero, P.J. de Pablo and A. Raman, *Proc. Natl. Acad. Sci. USA,* **2009**,*106*,13655.
22. S. Crittenden, A. Raman and R. Reifenberger, *Phys. Rev. B,* 2005, **72**,235422.
23. J. Legleiter, M. Park, B. Cusick and T. Kowalewski, *Proc. Natl. Acad. Sci. USA,* 2006,**103**,4813.
24. J. Melcher, X. Xu and A. Raman, *Appl. Phys. Lett.,* 2008,**93**, 093111.
25. I. Medalsy,U. Hensen and D.J. Müller, *Angew. Chem. Int. Ed.,* 2011, **50**, 12103.
26. F.Rico,C.Su and S. Scheuring,.Nano Lett., 2011, **11**,3983.
27. L.Picsa, F.Rico and S.Scheuring, *Biophys. J.,* 2012, **102**, L01.
28. R. Garcia and E.T.Herruzo,.*Nature Nanotech.,* 2012,**7**.217.
29. X. Xu, H. Melcher, S. Basak, R. Reifenberger and A.Raman, *Phys. Rev. Lett.*, 2009, **102**, 060801.
30. J.A.Turner and J. S.Wiehn, *Nanotechnology,* 2001,**12**, 322.
*31. O.Sahin, S. Magonov, C. Su, C. F. Quate and O. Solgaard, Nature Nanotechnol.,*2007,**2**,507.
32. R.Proksch, *Appl.Phys. Lett.*, 2006, **89**,113121.
33. S. Jesse, S. Kalinin, R. Proksch, A. Baddorf and B. Rodriguez, *Nanotechnology,* 2007, **18**, 435504.
34. N. F. Martinez, J. R. Lozano, E. T.Herruzo, F.Garcia, C. Richter, T.Sulzbach and R.Garcia, *Nanotechnology,* 2008,**19**,384011.
35. D.Martinez-Martin, E.T.Herruzo, C. Dietz, J. Gomez-Herrero, and R. Garcia, *Phys. Rev. Lett.*, 2011,**106**,198101.
36. M. Dong, S.Husale and O.Sahin, *Nature Nanotech*., 2009, **4**,514.
37. J. Legleiter, J.D.Fryer, D.M. Holtzman and T.Kowalewski, *ACS Chem. Neurosci.,* 2011, **2**, 588.
38. B.Kumar, P. M. Pifer, A. Giovengo and J. Legleiter, *J. Appl. Phys.,* 2010,**107**,044508.
39. M. P. Nikiforov, S. Hohlbauch, W. P.King, K.Voĭtchovsky, S. A. Contera, S. Jesse, S.V. Kalinin and R. Proksch, *Nanotechnology,* 2011,**22**,055709.
40. D.Martinez-Martin, C.Carrasco, M. Hernando-Perez, P.J.de Pablo, J. Gomez-Herrero,et al., *PLoS One,* 2012, **7**, e30204.
41. A.Dulebo, J. Preiner, F. Kienberger, G. Kada, C. Rankl, L.Chtcheglova, C.Lamprecht, D. Kaftan and P. Hinterdorfer, *Ultramicroscopy,* 2009, **109**,1056.
42. A.Raman, S.Trigueros, A. Cartagena, A.P.Z.Stevenson, M.Susilo, E.Nauman and S.A.Contera, *Nature Nanotech.,* 2011, **6**,809.
43. R.D.Turner,J.Kirkham, D. Devine and N.H. Thomson, *Appl. Phys. Lett.,* 2009,**94**, 043901.
44. Müller,D.J.; Engel, A. *Nature Protocols* 2007,**2**,2191.
45. Dong, M.; Sahin,O. *Nature Commun.* 2011, **2**, 247.
46. M.P.Mingeot-Leclercq, M. Deleu R.Brasseur andY.F.Dufrêne, *Nature Protocols,* 2008, **3**,1654.
47. G. Zaccai, *Science,* 2000, **288**, 1604.
48. H. Luecke, B. Schobert, H. T. Richter, J. P. Cartailler and J. K. Lanyi, *J. Mol. Biol.*, 1999, **291**, 899
49. S. Zhong, H. Li, X. Y. Chen, E. H. Cao, G. Jin and K. S. Hu, *Langmuir*, 2007, **23**, 4486.
50. A. F. Payam, J.R. Ramos and R. Garcia, *ACS Nano,* 2012,**6**, 4663.